Proceedings of ASME Turbo Expo 2013
GT2013
June 3-7, 2013, San Antonio, Texas, USA

GT2013-94478

An Experimental Study of Mist/Air Film Cooling On a Flat Plate with Application to Gas Turbine Airfoils- Part 2: Two-Phase Flow Measurements and Droplet Dynamics

Lei Zhao and Ting Wang
Energy Conversion and Conservation Center
University of New Orleans
New Orleans, LA 70148-2220, USA
Emails: leizhao.me@gmail.com; twang@uno.edu

ABSTRACT

A Phase Doppler Particle Analyzer (PDPA) system is employed to measure the two-phase mist flow behavior including flow velocity field, droplet size distribution, droplet dynamics, and turbulence characteristics.

Based on the droplet measurements made through PDPA, a projected profile describing how the air-mist coolant jet flow spreads and eventually blends into the hot main flow is proposed. This proposed profile is found to be well supported by the measurement results of the turbulent Reynolds stresses. The coolant film envelope is identified with shear layers characterized by higher magnitudes of turbulent Reynolds stresses. In addition, the separation between the mist droplet layer and the coolant air film is identified through the droplet measurements—large droplets penetrate through the air coolant film layer and travel further into the main flow.

With the proposed air-mist film profile, the heat transfer results on the wall presented in Part 1 are re-examined and more in-depth physics is revealed. It is found that the location of optimum cooling effectiveness is coincided with the point where the air-mist coolant stream starts to bend back towards the surface. Thus, the data suggests that the "bending back" film pattern is critical in keeping the mist droplets close to the surface, which improves the cooling effectiveness for mist cooling.

NOMENCLATURE

l	chord length (mm)
M	blowing ratio, $(\rho u)_j/(\rho u)_g$
Re	Reynolds number
T_{aw}	adiabatic wall temperature (K)
T_w	wall surface temperature in contact with gas (K)
T_g	main gas flow temperature (K)
T_j	coolant temperature at the cooling jet hole exit (K)
T_u	turbulence intensity

Greek Letters

η	adiabatic film cooling effectiveness, $(T_g-T_{aw})/(T_g-T_j)$
$\overline{uv}$	Reynolds stress

Subscripts

f	air film cooling
g	main flow of hot gas/air
m	mist/air film cooling

INTRODUCTION

In these two-part papers, Part 1 is focused on the heat transfer result on the wall and Part 2 will be focused on the droplet multiphase flow behavior.

Particle (water droplets) measurement is an important part in understanding the fundamental mechanisms of mist cooling since the particle sizes, particle evaporation, particle dynamics, and their distribution play an essential role in determining mist film heat transfer and cooling effectiveness. Chaker et al. [1] conducted droplet measurements using a Malvern system in the effort to study gas turbine inlet fogging. Young and Bachalo [2], Dodge [3], and Le Coz [4] compared the droplet measurement results using different systems in their separate studies.

A Phase Doppler Particle Analyzer (PDPA) system, invented by Bachalo in the 1980's [5], is used in this study. The PDPA Method is based upon the principles of light scattering interferometry. Two collimated, monochromatic, and coherent laser beams are made to cross at a point (measurement point), where they interfere and generate light fringes. A particle moving across the fringes will reflect light, which is picked up by a receiving lens located at a certain off-axis collection angle. A set of (usually 3) detectors in the receiver is used to capture the signals. The temporal frequency of the signal is used to determine the particle velocity, and the spatial frequency can be used to calculate the particle size. It is noted that one distinguished feature of PDPA measurement, compared with conventional interferometric techniques such as Laser Doppler Anemometry (LDA), is that the change in phase is independent of the incident intensity or scattering amplitudes of light, but is directly proportional to the droplet diameter. PDPA measures the relative phase shift of the Doppler signal directly as a linear function of the droplet diameter. As such, PDPA measurements are dependent on the wavelength of the scattered light, which is not easily affected by environmental conditions. This feature gives PDPA measurement a clear advantage over the conventional intensity-based measurement method which is sensitive to background noise.

Another noted feature of the PDPA system is that its detector is commonly placed off the plane of the transmitting beams at an angle close to 30^o. This is because the intensity of the scattered light, which affects the Signal-to-Noise Ratio

(SNR), can vary by several orders of magnitude depending on the receiving angle and the droplet concentration. Generally, within the angle of 0º-20º off the transmitting axis, light is scattered primarily by diffraction, which contains no information for the PDPA process. At an angle between 20º-90º, which is called the forward-scattering region, the scattered light, mostly by refraction for non-opaque droplets, has the highest SNR, thus the size sensitivity is the best. 30º forward-scattering is adopted in this study due to the special need to receive the strongest signal at about 30º (due to light refraction caused by particle with certain sizes).

Guo, et al., [6,7] employed a PDPA system to measure the water droplet dynamics in a mist/steam cooling study in a heated tube and 180º-bend tube with an application to closed-loop steam cooling for H-type gas turbines. Wang et al. [8] and Li, et al., [9-11] used the same PDPA system to investigate mist/steam impinging jet schemes to augment gas turbine airfoils cooling performance. The PDPA system used in this study is a product of TSI Inc.

EXPERIMENTAL SETUP

The PDPA system used in this study has a fiber-optic probe with a focal length of 350 mm and a beam waist diameter of 115 μm. The beam spacing for the probe is 50 mm. The focal length of the receiver for the PDPA system is 500 mm. The laser system is an Argon-Ion type water cooled system with 4 Watts maximum power output. The wave length used in the system is 514.5 nm (green) and 488.0 nm (blue). A typical value of 36-40 MHz downmixing is used for this study together with the band pass filtering range of 1 to 10 MHz. The particle data is filtered with a high PMT (Photomultiplier Tube) voltage of 1000 mV. Since the scattered light intensity is proportional to the square of the particle diameter, the d^2-law is applied to the high PMT filter curve. The d^2 law is based on the geometrical optics and does not apply to very small particles, and, thus, a low value of 0.1–0.2 mV is applied for the low threshold value.

Droplet Measurement

The PDPA measurements are verified against Polymer Latex particles (manufactured by Duke Scientific Corp.) of known-sizes. These particles, with moderately low standard deviations for a given size, are microspheres with a density of 1.05×10^3 kg/m^3 and a light refraction index of 1.59 at 590 nm. The verification process is performed by putting the Polymer Latex particles into a container made of the acrylic sheet with the same thickness as the test section wall. By doing so, the plastic window effect on the particle measurement as that would be included during the real test section measurement will be evaluated. The container is filled with water and the particles are suspended in the liquid. A small propeller driven by a mini-motor is immersed in the container. The purpose of the small propeller is to induce particle motion in the water so that a certain number of particles can be captured passing through the measurement volume to generate enough data in the PDPA measurement system in a given amount of time to satisfy a statistical requirement. Three different particle sizes are used. Figure 1 shows the result of the PDPA measured particle sizes compared with the true particle sizes. It can be seen that in the size range of 2~40 microns, the measured particle sizes from PDPA agree well with the actual particle sizes within ± 4%. It is noted that the container wall (made of acrylic sheets) does not have a significant effect on particle size measurements.

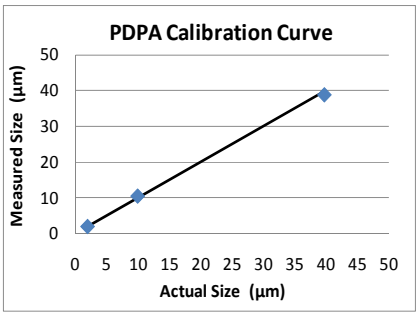

Figure 1 Calibration of the PDPA measurement with the mono-sized polymer latex particles

A detailed description of the experimental setup and particle measurement process is documented in a companion paper [12].

RESTULS

Review of Heat Transfer Results

Through the investigation of the heat transfer results in Part 1, it is found that the general pattern of the adiabatic cooling effectiveness distribution of the mist case is similar to that of the air-only case with the peak at about the same location. This implies that adding mist in the air film does not change the general cooling pattern drastically, so that knowledge acquired through film cooling can generally be applied to mist cooling.

For the 0.6 blowing ratio case, the cooling effectiveness is greatly enhanced. The net enhancement of adiabatic cooling effectiveness compared to the air film case reaches 190% locally and 128% overall at the centerline, the cooling coverage is increased by 83%, and a more uniform surface temperature is achieved. The latter is critical for reducing wall thermal stresses. When the blowing ratio increases from 0.6 to 1.4, both the cooling coverage and net enhancement decreases to below 60%.

For M=0.6 case, it is noted that the momentum flux ratio is 0.37 for the continuous phase (air). Considering the added overall weight due to liquid phase (thus the higher density of the mixture), the momentum flux ratio is 0.40.

It is noted that for the high blowing ratio cases with coolant being lifted off of the surface, mist cooling makes the stream-wise surface temperature gradient steeper, which may raise a concern for increased thermal stresses. Therefore, it is more beneficial to choose a relatively low blowing ratio to keep the coolant film attached to the surface when applying the mist cooling. The centerline integral of net enhancement for M = 1.4 is only 11.4%, which is the lowest for all three of the blowing ratios tested.

For easier reference in the following discussion of droplet measurements, the heat transfer result plots of the M = 0.6 cases are shown again in Figs. 2 and 3. The improved lateral cooling after mist is injected is believed being attributed to the 3-D kidney and anti-kidney vortices generated by the round film hole. It is hypothesized that the double vortices could help to spread the mist droplets wider than the air in the lateral direction and thus generate the much better cooling pattern

across the holes –comparing Fig. 2(a) with (b). However, we didn't gather sufficient droplet data in the double vortices to validate this hypothesis.

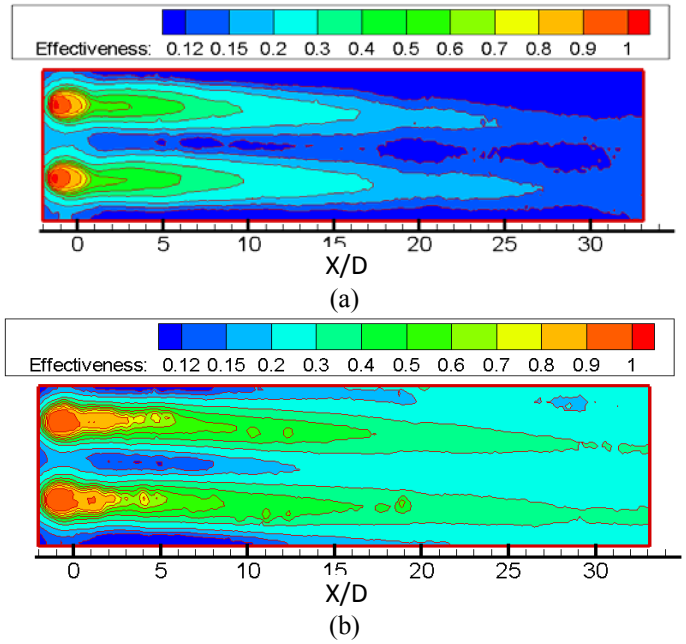

Figure 2 Contour of cooling effectiveness for (a) Case 1, M=0.6, air-only film (b) Case 2, M=0.6, mist/air film

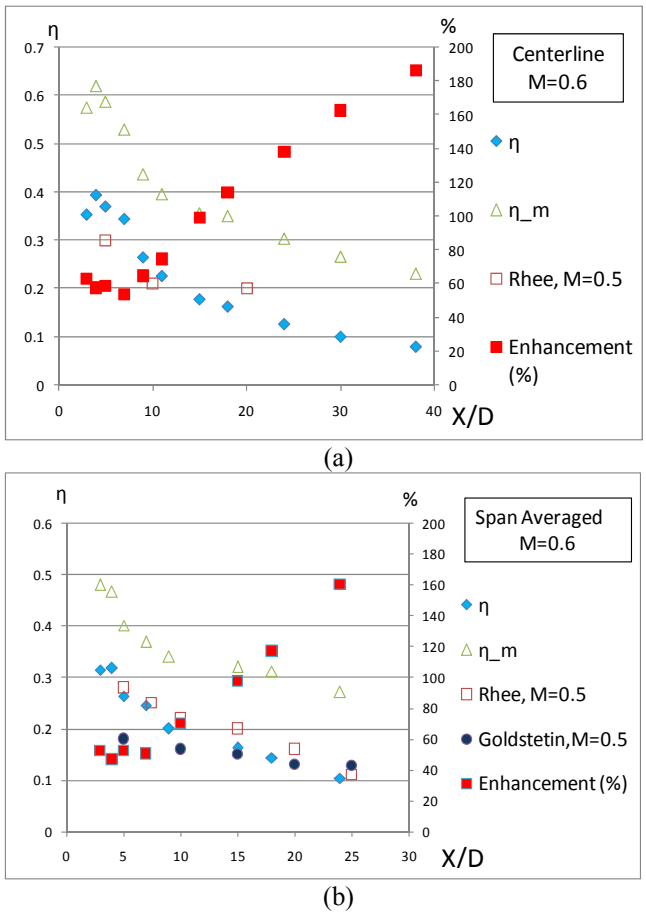

Figure 3 Comparision of present adiabatic cooling effectiveness (left coordinate) and net enhancement (right coordinate with the experimental data from Goldstein et al. and Rhee et al. (a) M=0.6, centerline data (b) M=0.6, spanwise averaged data

Droplet Measurement Results

To understand the mist cooling heat transfer results, an understanding of the droplets behavior and their interactions with the flow field and temperature field is essential. The PDPA system is employed to measure the particle information. The interested measurements include droplet size distribution, velocity, and droplet population density. The droplet velocity includes the instantaneous velocity and the averaged velocity in both the stream-wise and cross-stream (perpendicular to the wall) directions.

The PDPA measurement is essentially a point measurement method. It documents the particle that passes by the specific point of measurement. Traversing of the laser beams is needed to map out the information in a plane or space to give a more general picture of the whole field. This requires a lot of time and effort to accomplish, and, as a result, the spatial resolution is limited to the number of measurement points.

The particle signal is random in nature. A certain number of samplings is needed to give meaningful measurements. As a result, all of the measurement data needs to be treated in a statistical manner. Interpretation of the data also requires an understanding of the random nature of the data. For example, the Fourier Transform for the random data is very different from that of a continuous measurement sampled with equal periodicity. Some assumptions need to be made to perform the Fourier Transform analysis over scattered and non-periodic data.

Droplet Size Distribution Plots

The distribution of droplet sizes for the case where M = 0.6 is shown in Figs. 4-7 at different stream-wise locations. Within each figure, the particle size distribution at different elevations (Y-axis) from the surface is plotted. The X-axis is the particle size and the Y-axis is the particle data rate. Those figures are intended to give the information of the particle size distribution over the flow field. Particle size information is critical in understanding the droplets' behavior and the evaporation process in mist cooling. It has close interactions with the thermal-flow field. Also, the variation of droplet size reveals the heat transfer characteristics of mist cooling.

The particle data rate is the number of particles that are captured and counted per unit time at the measurement location. It is noted that not all of the particle signals are counted in the measurement: only the signals that meet certain threshold criteria. For example, the intensity of the light that is reflected by a particle is theoretically proportional to its size, i.e. bigger particles reflect higher intensity light while smaller particles reflect lower intensity light. Thus, if a particle's signal bears very low light intensity, but still appears quite large in size based on the frequency measurement, the signal will be dropped because it is very likely that the light signal is from wall reflection or is simply noise.

The particle data rate is determined by a combination of two factors: particle velocity and particle density. As particle velocity increases, more particles pass the measurement volume per unit time, and, as a result, the particle data rate is higher. Similarly, if the particle distribution is dense in the area, more particles will be captured per unit time, also resulting in higher data rates.

Mean Droplet Sizes. The most important droplet characteristic is the mean diameter. This diameter can be evaluated in various ways. The most commonly used mean diameter is the arithmetic mean diameter (D_{10}). Other commonly used mean diameters are the area mean diameter (D_{20}), volume mean diameter (D_{30}), and the Sauter mean diameter (D_{32}), which represents the ratio of volume to area. If all the droplets are of the same size, then $D_{10} = D_{20} = D_{30} = D_{32}$. For droplets with different sizes, D_{10} among all the mean diameters has the smallest value, while D_{32} has the largest. Generally, D_{10} represents the diameters of the most droplets, D_{32} represents the diameters of large droplets. For example, if we have 100 spherical droplets with 90 of them having diameters of 1, and 10 having a diameter of 10, then D_{10} = 1.9, D_{20}=3.3, D_{30}=4.7, and D_{32}= 9.3. The data of all the diameters are provided in Figs. 4-7, but only D_{10} is used for analysis in this paper for simplicity.

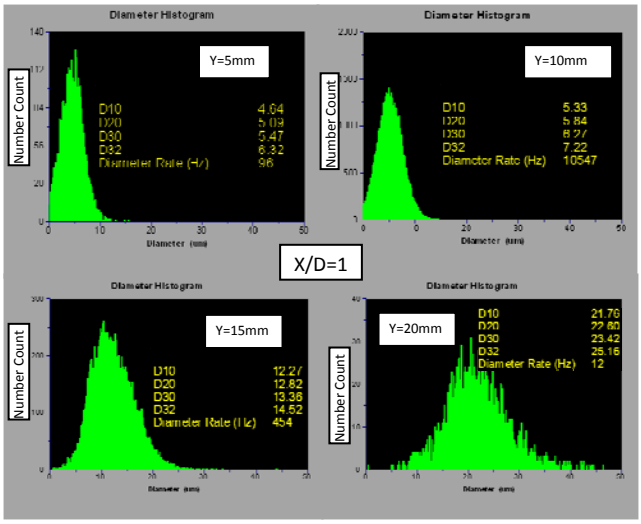

Figure 4 Droplet size distribution of various y locations at X/D=1, M=0.66

In the area very close to the injection hole, X/D = 1, as shown in Fig. 4, the droplet distribution of different Y-elevations is plotted. Notice that the droplet distribution patterns at Y = 5mm and 10mm are quite similar. The droplet size distribution is centered at about 5μm and the biggest droplets are sized at 15μm. The difference is that the droplet data rate at y = 10mm is one scale higher than that of y = 5mm. As a result, the curve of y = 10mm looks smoother than that of y = 5mm. As the measurement elevates to y = 15mm, the droplet distribution changes greatly with the most frequently captured droplet size increasing to about 12μm with the largest droplets sized at 30μm. Droplets that are smaller than 10μm only account for less than 5% of the total droplet population. It is noted that the particle number counts (within the same time interval) shown on the Y-axis reduce to about the same level as y = 5mm. As the Y-coordinate further increases to 20mm, the most frequently captured size increases to 21μm and the biggest droplet can be as large as 40μm or larger. Meanwhile the droplets smaller than 10μm almost disappear at this elevation level. It is noted that the droplet data rate is very low too.

In summary, at an area very close to the injection hole, X/D = 1, the particle size distribution moves towards larger sizes away from the surface. The particle data rate increases first from 5mm to 10mm away from the surface, and then decreases to zero at higher Y-elevations.

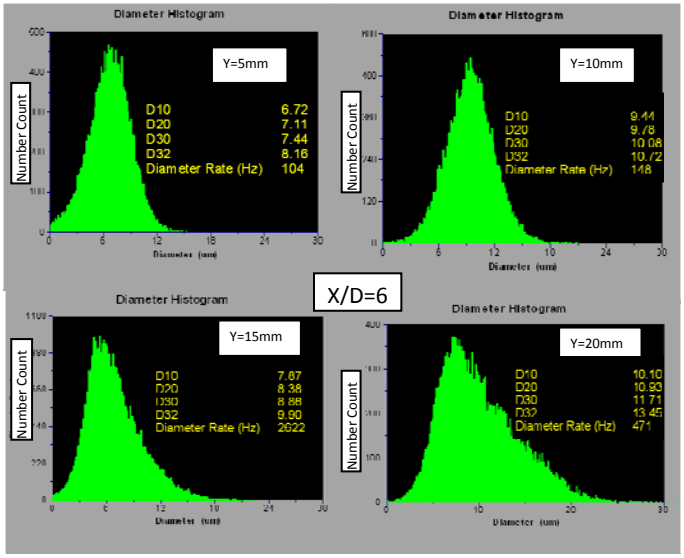

Figure 5 Droplet size distribution of various y locations at X/D=6, M=0.66

As X/D further increases (i.e. moving downstream), the particle size distributions at the same elevations at X/D = 6 are plotted in Fig. 5. At Y = 5mm, compared to the same plot at X/D = 1, the size distribution leans towards bigger sizes, with the most frequently captured size being 7μm (compared to 5μm for X/D = 1 at 5mm). Correspondingly, the largest size reaches 17μm. The smaller particles make up a smaller portion of the total particle population. At Y = 10mm, the size distribution leans towards bigger sizes compared to those at Y = 5mm with the most frequently captured size at 10μm. An interesting observation can be seen when the comparison is made between the distributions at Y = 10mm and 15mm. The center of the droplet size distribution moves towards smaller droplets, decreasing from 10μm to about 6μm. This is opposite to the trend found for X/D = 1. At Y = 20mm, the droplet size increases again. So, looking from bottom to top, the droplet size first increases, then decreases slightly, and eventually increases again. This is one of the interesting characteristics of the droplet distribution pattern involving film jet flow with particles. It is a combined effect of the droplet interactions within the flow and temperature fields. Detailed investigation and interpretation of these phenomena and their effects on surface heat transfer will be discussed after more information about the particles is presented.

As X/D further increases to 13, it is found in Fig. 6 that, at Y = 5mm, the data rate is very low and the size distribution curve is not as smooth due to the small amount of sampling data. The data rate increases significantly at Y = 10mm showing a smooth, symmetric distribution curve centered with the 7μm droplets as the most frequently captured size and ending with the biggest size at about 18μm. At Y = 20mm, the droplet size distribution leans towards bigger droplets and the data rate is very low, while the size distribution is no longer symmetric as in the lower elevation levels. This means that bigger droplets are more frequently present at this measurement point.

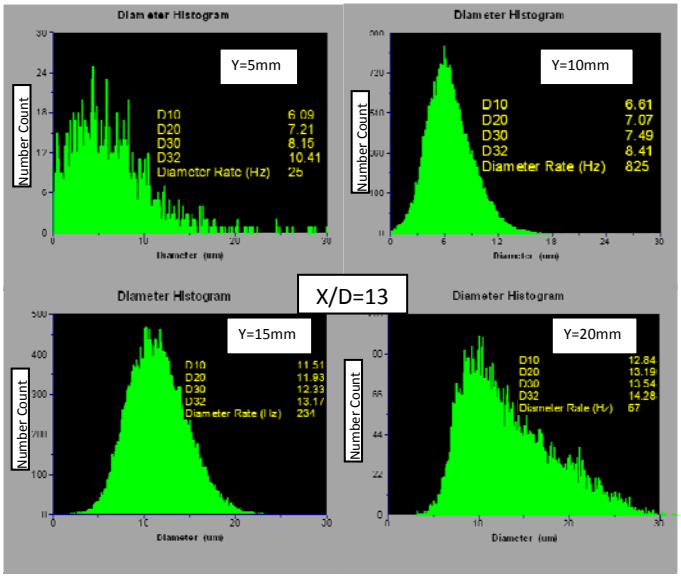

Figure 6 Droplet size distribution of various Y locations at X/D=13, M=0.66

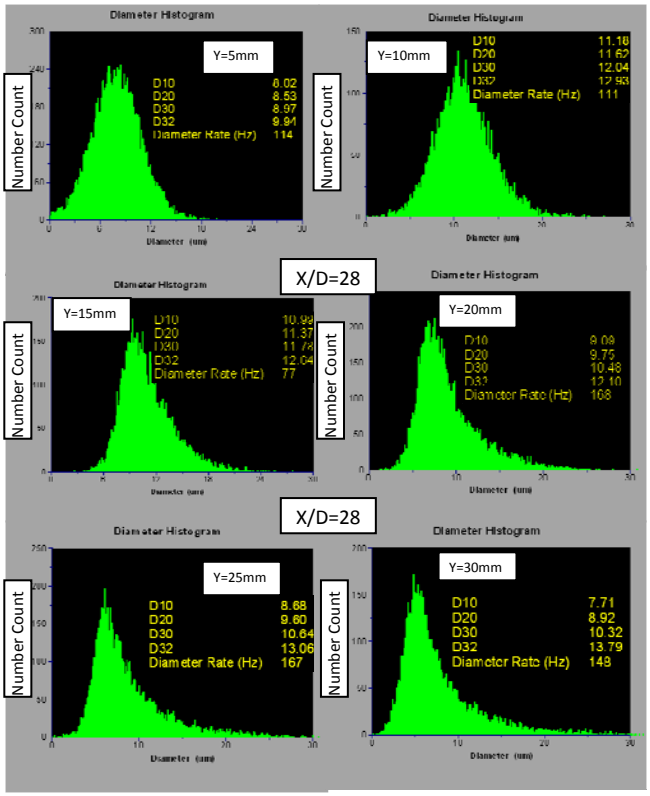

Figure 7 Droplet size distribution of various Y locations at X/D=28, M=0.66

In the region far away from the injection hole, X/D = 28, shown in Fig. 7, the particle size distributions at Y = 5mm and 10mm are both almost symmetric with the average size at Y = 10mm being bigger than that at Y = 5mm. This distribution is quite similar to that of the upstream locations. One interesting finding is that at elevations of Y = 20mm and higher, the size distribution is almost identical. The plots have similar shape, the average size is about the same, and the droplet size distribution leans towards bigger particles. It should also be noted that the particle data rates are similar. Assuming that this height is outside the boundary layer and inside the core of the main flow (which proved to be true later), the speed of the droplets is almost the same. Since the data rate is determined by the particle density and speed, it is concluded that the droplet density is also similar in this region. Thus, this information shows that, beyond a certain height away from the surface, the droplets have a similar size distribution, density, and speed. This is interpreted to mean that, at the elevations beyond Y = 20mm, the droplet distribution is not a function of elevation any more.

Size Distribution with Particle Data Rate Plots

In order to give more detailed information about the droplet behavior, the average droplet size distribution is plotted together with the droplet data rates in Fig. 8. By putting them together in the same plot, some correlation patterns are expected to be revealed.

The average droplet size as a function of the vertical distance from the surface is plotted in Fig. 8 for different stream-wise locations. On the chart, the X-axis is the vertical distance (Y) from the plate surface and the Y-axis on the left is the average droplet size. Four stream-wise locations, X/D = 1, 6, 13, and 28 are plotted in Fig. 8 (a), (b), (c), and (d), respectively. The data rates are plotted on the secondary Y-axis on the right.

Looking at the average droplet size (D10) distribution for X/D = 1, the first measurement point is 6 mm away from the surface. Note that, below this point, the data rate is too low to produce a meaningful measurement. This means that there is a very minimal number of droplets present under a certain elevation from the surface. From a real physics point of view, this result shows that the droplets are actually lifted away from the surface at the area very close to the injection hole (X/D = 1). This is understandable because mist droplets are carried into the main flow chamber by the coolant. With the help of the initial coolant jet's injection momentum, droplets will be lifted off. The average droplet size is almost constant (5 μm) from 6 mm to 12 mm away from the surface. The average droplet size suddenly starts to increase from Y = 12 mm to reach 27 μm at Y = 22 mm. Again, it is noted that beyond Y = 22 mm, the data rate is too low for any meaningful measurements. This indicates that the droplets are almost absent beyond Y = 22mm. This is also understandable from the physics point of view that the momentum of the droplets acquired from the coolant jet is not strong enough to shoot the droplets this high. Also, the particle distribution information rules out the possibility that the absence of droplets anywhere higher than Y = 22 mm is caused by complete evaporation at this height, because the droplet size is actually increasing away from the wall below this point. Therefore, the reason for the low droplet count beyond a certain height is mainly caused by the fluid mechanics, not the heat transfer. It can be concluded that fluid mechanics is the dominant factor that determines the droplet size distribution.

At X/D = 1, it is noticed that there is a small "hump" (local maximum) in the droplet size distribution curve at around Y = 7mm. Due to the measurement uncertainty, which is estimated as high as 5%, it is not clear whether this "hump" is real or not from this figure alone.

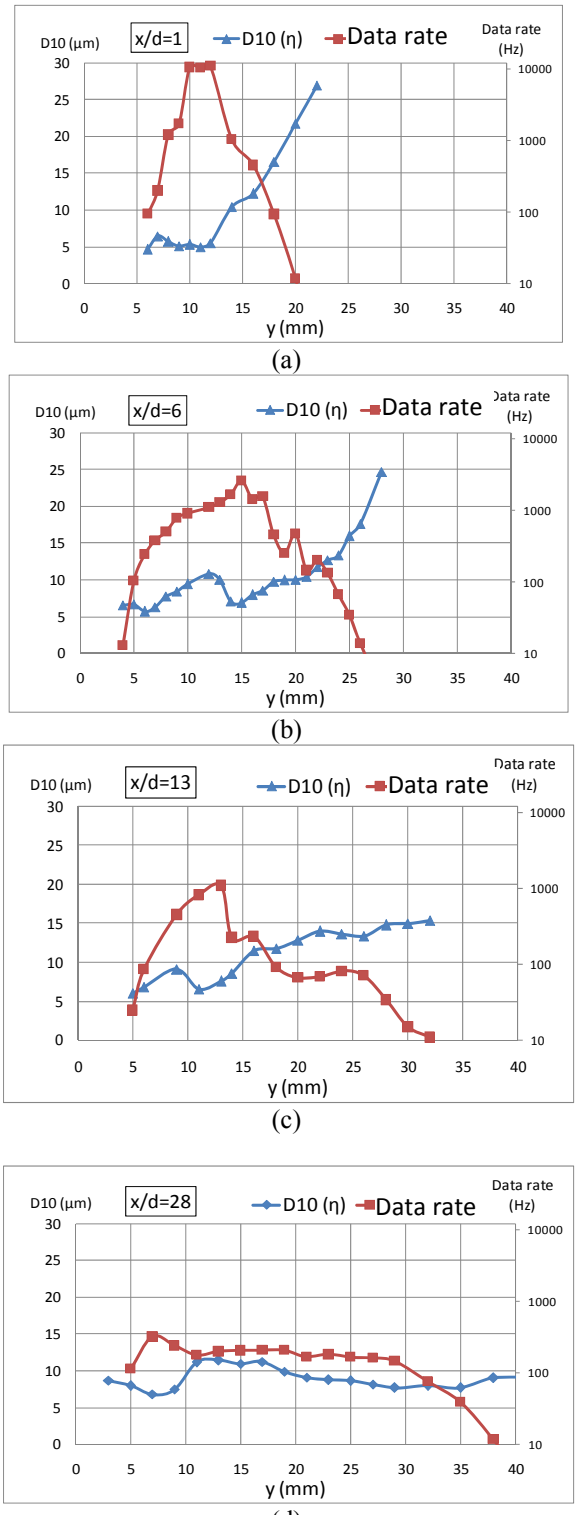

Figure 8 Case 2 (M=0.6) particle size distribution (on left Y coordinate) and particle data rate distribution (on right Y coordinate) as a function of Y locations at (a) X/D=1 (b) X/D=6 (c) X/D=13 (d)X/D=28

Examining Fig. 8 (b) at X/D = 6, the general pattern of D_{10} increasing as Y increases is followed. But, this figure shows many other interesting patterns that can be more clearly seen by comparing it with the D_{10} distribution in Fig. 3.8 (a). The results of comparison are summarized as follows:

- In the region of Y < 6mm at X/D = 6, the average droplet size is relatively small at about 6 μm. Similar to the size distribution at X/D = 1, the droplet size is almost constant within this area, but slightly bigger than the corresponding size distribution at X/D = 1.
- In the next region of 6 mm < Y < 15 mm, a "hump" is seen in the D_{10} distribution at Y = 12 mm. Within the "hump," the average droplet size first increases to about 11 μm at Y = 12 mm and then decreases to about 7 μm at Y = 15 mm.
- It is noted that the slope of the left side of the "hump" is smaller than that on the right side. This means that the droplet size increases slowly toward the peak as Y increases and then decreases quickly away from the surface.
- In the region beyond Y = 15 mm, the droplet size continues increasing to reach about 24 μm at Y = 25 mm.

In summary, the size distribution can be roughly characterized in three sections: the flat curve section with Y < 6 mm, the "hump" section with 6 mm < Y < 15 mm, and the outside "hump" section with Y > 15 mm.

Now looking at Fig. 8 (c) at X/D = 13, the D_{10} distribution pattern is similar to that of Fig. 8 (b). But the differences are:

- The flat curve section is not obvious.
- The location of the "hump" moves closer to the wall for 5 mm < Y < 12 mm.
- The "hump" is smaller compared to X/D = 6 with the peak value of D_{10} about 9 μm.
- The droplet size outside the "hump" is smaller compared to the size within the same region (outside of hump, not necessarily the same Y values) of the X/D = 6 case. The largest D_{10} is 15 μm compared to the 24 μm of the X/D = 6 case.
- The size (D_{10}) distribution at X/D = 28 is quite different from the previous cases. The "hump" pattern is not recognizable. Droplet size slightly decreases from Y = 2.5 mm to Y = 7 mm and then sharply increases starting above Y = 7 mm. In the region higher than Y = 20 mm, the average size changes only slightly.

Physical interpretation of those distribution patterns is very important in understanding the mist cooling mechanisms. Before making any judgment or conclusion based on the size distribution plots, the particle data rate distribution will be examined as well, which is expected to help in the interpretation of the data.

Again, the particle data rate is the number of particles that are captured and counted per unit time at the measurement location. Since the particle data rate is affected by both the particle velocity and the density, in order to simplify the analysis, it is first assumed that the droplet velocity does not significantly affect the particle data rate. The validity of this assumption will be re-examined later. With this assumption made, the particle data rate can now be interpreted to be directly proportional to the droplet's density.

The particle data rate is plotted on the Y-axis on the right in Fig. 8 (a), (b), (c), and (d) for different X/D locations of 1, 6, 13, and 28, respectively. The X-axis is the vertical distance from the plate surface. The data rate, due to its high variation in scales, is plotted on a log-scale. Examining Fig. 8 for data rate plot for different X/D locations, it is found that a roughly

conical shape is observed in all four plots. This shape is not as obvious for the X/D = 28 case as it is in the other three cases, but it is still recognizable. In general, the particle data rate increases first and then decreases, with some exceptions locally at small scales. *In a nutshell, there exists an "envelope" of air containing the droplets within the flow. All droplets are distributed only within the "envelope," which is characterized by an apex showing the highest droplet density and bounded by upper and lower elevations. Outside this envelope, the droplet density quickly drops to almost zero.* A first impression is that this envelope might represent the trace of the film jet's width. But, a further analysis renders this initial impression questionable because: if the "envelope" were the jet film, the existence of many patterns of the droplet size distribution in this envelope could not be convincingly explained. It appears more in-depth analysis is required.

One important observation by considering both the size distribution and the data rate together is that the peak location of the particle data rate is always in the close neighborhood of the location where the droplet size starts to increase "on the right side of the hump"--- a local minimum. In other words, the location of the peak of the data rate "envelope" is always close to the right boundary of the "hump." The values of the locations acquired corresponding to the peak of the data rate curve and the "hump" right boundary of the droplet size curve are summarized in Table. 3. As shown in the table, the Y-locations corresponding to the peak in the data rate curve and the right side of the "hump" in the droplet size curve are almost identical except for a slight difference at X/D = 13.

Table 3 Comparison of the Y location for coolant film upper boundary acquired from the data rate curve and the size curve (Case 2, M=0.6)

x/d	size curve (mm)	data rate (mm)
1	11.0	11.0
6	15.0	15.0
13	11.0	13.0
28	7.0	7.0

The Proposed Coolant Air/Droplet Spreading Profile in the Cooling Film

The physics of the aforementioned observations is summarized below:

- The coolant film, mixed with the mist droplets, keeps its own identity traveling in the main flow channel in the area of 1 < X/D < 13 in the stream-wise direction. The coolant film with mist travels as a layer with finite thickness, which is discernible through the combined information of both the size curve and the data rate curve.
- The right side of the "hump" in the droplet size curve indicates the upper boundary of the coolant jet layer. This upper boundary can also be identified by the location of the peak value from the data rate curve.
- The bottom boundary of the film cannot be identified as clearly as the upper boundary. However, the bottom boundary can be roughly estimated by the location where the data rate is lower than 50 Hz on the left side of the "hump." The difference between the two is not significant, and the shapes of the curves are similar, which will be shown later in this section.
- The size of the "envelope", as shown by the data rate curve, is the range where the droplets can reach. It is noted that this envelope size is larger than the film layer width. However, the width of the "hump" corresponds to the width of the jet film.

Based on the proposed profile of coolant air film, another important observation is made that there is a separation between the coolant air film (mixture of cooling air and droplets) and the droplet layer (within which droplets reside). The two layers do not coincide. In other words, large droplets penetrate through the air coolant film layer and travel further into the main flow. This phenomenon was observed in CFD simulations as well and was reported by the studies of Li and Wang [12, 13].

Supporting Data for the Proposed Coolant Air/Droplet Spreading Profile

It is noted that after the peak value in the data rate curve, the data rate decreases sharply for all cases in Fig. 8. Based on the assumption that the data rate is directly proportional to the droplet density, this implies that the droplet density decreases sharply after the peak. From the previous assumption for easier analysis, the coolant film still keeps its identity and travels in a layer of spreading finite thickness. Also, the peak of the data rate curve is right on the boundary of the coolant film layer. Thus, the right side of the peak of the data rate curve is actually outside the span of the coolant film. Noting that the mist is injected into the main flow channel carried by the coolant film, it makes sense that number of droplets decrease sharply outside the coolant film layer. The data rate decreases quickly outside the coolant film carrying the most mist. Water droplets, with a higher density than air, tend to shoot higher than the air coolant film. Thus, the droplet population density is higher toward the top boundary of the coolant jet. Another minor reason for the data rate going higher toward the top boundary is that the air flow speed is slightly higher on the top of the film and approaches the main flow speed, so more droplets pass the measurement location during the observation time, resulting in a higher data rate. Overall, two observations are concluded: *(1) inside the film layer, the data rate goes higher because of the fact that fluid mechanics determines the distribution and (2) the data rate starts to decrease at the film's top boundary. Thus, the peak can only exist at the top of the boundary as a natural result of 1 and 2*.

On the other hand, if the droplets can travel outside of the coolant film layer, they must possess momentum that is high enough to break through the coolant film layer. Due to the long distance that the droplets have traveled through in the mixing chamber, it is believed that the droplets have reached their terminal speed (i.e. the droplets maintain a constant slip velocity with the coolant air.) before entering the film hole. As a result, bigger droplets will have higher initial momentum shooting into the main chamber because the droplets are accelerated though the film hole channel from the coolant supply plenum. Bigger droplets have higher mass, and, thus, higher momentum. Therefore, the droplets that are able to acquire enough momentum to break through the coolant film must be "big" droplets. Now, from the series of analyses conducted above, it is concluded that this feature of bigger

droplets existing outside the coolant film stream should be reflected in the size distribution curve. Indeed, this feature is actually shown clearly in the size curve. As discussed previously, outside the "hump," the average droplet size increases with the elevation. Thus, combining the information from the size curve and the data rate curve, the particle and flow physics, it is concluded that *the location where the data rate starts to decrease is exactly where the droplet size begins to increase as the upper boundary of the film stream.*

As discussed in the previous section, the initial droplet size distribution is determined mainly by fluid mechanics rather than heat transfer. The bigger the droplets are, the higher their momentums are, and, in turn, the further up those big droplets can travel to. This explains why the droplet size increases as Y elevates. And, due to those big droplets, which are able to break through the coolant film layer, the size (width) of the "envelope" in the data rate curve is bigger than the size (width) of the "hump."

As for the bottom boundary of the coolant film layer, it cannot be easily measured due to the fact that the gap between the coolant film and the test surface is in the scale of millimeters. The droplet density in this area is very low and not enough measurement points are available. As a result, there is no significant pattern from either the droplet size curve or the data rate curve that can clearly identify the jet stream lower boundary. However, rough estimates could be made by extrapolating the data rate curve to the location where zero data rate would occur or by identifying the left boundary of the "hump" in the droplet size curve. Both estimates are very rough and uncertain. The locations of the lower boundary of the jet stream obtained by using these two rough approaches are presented in Table 3.4.

Table 4 Comparison of the Y-location for coolant film lower boundary acquired from the data rate curve and the size curve (Case 2, M=0.6)

x/d	size curve (mm)	data rate (mm)
1	6.0	3.0
6	6.0	4.5
13	5.0	4.0
28	2.0	2.5

In order to further investigate the relationship between the droplet size distribution and coolant stream boundaries, the turbulence Reynolds stress ($\overline{uv}$) is plotted on the secondary Y-axis in the same figure of the size distribution curve in Fig. 9.

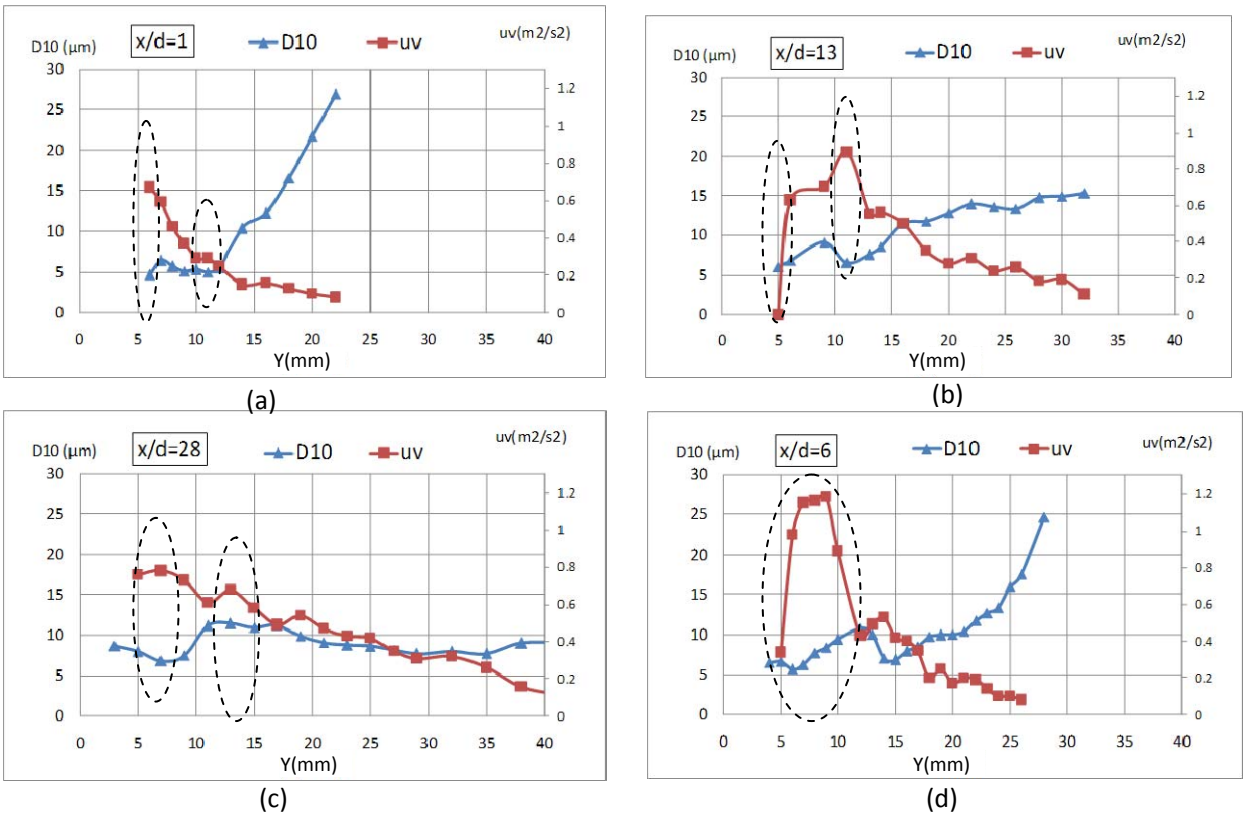

Figure 9 (Case 2, M=0.6) Droplet size distribution (plotted on Y-coordinate on the left) and Reynolds Stress distribution (plotted on Y-coordinate on the right) as a function of Y-locations at (a) X/D=1 (b) X/D=6 (c) X/D=13 (d)X/D=28

The turbulence Reynolds stress is expected to be higher in the shear layer between the coolant film layer and the main flow. Looking at Fig. 9, the locations of the peak of the Reynolds stress show reasonable agreement with the left and right boundary of the "hump." The corresponding patterns are circled in each figure. Even though some of the patterns are not clearly identifiable, the corresponding patterns are still discernable in most of the cases. Therefore, based on the droplet's data count and the maximum Reynolds shear stress, the edges of the hump of the droplet size curve coincides with the upper and lower boundary of the jet's width.

Now the assumption made earlier that the droplet velocity will not affect the data rate needs to be examined. The average particle velocity (U) is plotted on the right Y-axis in the same figure of the size distribution curve in Fig. 10.

Further Explanation of Droplet Distribution

According to the previous analysis from a fluid mechanics point of view, the right end of the "hump" of the droplet size curve is the upper boundary of the coolant jet film and the left end of the "hump" is approximately the lower surface of the film layer. In other words, the width of the "hump" is roughly corresponding to the width of the coolant jet film. The profile of the "hump" indicates that the biggest droplets are in the middle of the film layer and the droplet sizes decrease from the center towards both sides of the film layer. This can be explained that heat transfer becomes high near the jet stream boundaries, so the droplet sizes diminish towards the boundaries. On the upper boundary, the droplets are directly exposed to the hot main stream flow, and on the lower boundary, the droplets are also exposed to a relatively hot flow which results from the 3-D flow wrapping the main flow around the sides via the lateral vortices. Thus, the droplet size becomes smaller as it approaches the surface.

Combining the explanation for both the upper and bottom surface boundaries of the air/mist film, there is a cold core inside the film. The droplet sizes are bigger inside this cold core due to the less severe heat transfer, thus slower evaporation of the mist droplets.

It is observed previously in Fig. 8 that for the X/D = 6 case, the slope of the droplet size curve is different on both sides of the "hump." Droplet sizes decrease faster towards the upper boundary and decay slower towards the lower boundary. As a result, the peak size inside the film skews towards the upper boundary. This implies that the heat transfer rate from the upper surface into the coolant jet is stronger than that from the lower boundary.

Looking at the droplet size distribution curve at X/D = 1 and X/D = 6 in Fig. 8, inside the film layer, i.e. the "hump," the sizes for the X/D = 1 case are around 5μm. However, the droplet size for the X/D = 6 case reaches as high as 10 μm. This poses a tough question for the proposed profile to answer. If the mist droplets are contained in the mist/air film, as they travel from X/D = 1 to X/D = 6, they should absorb heat from the surrounding hot main flow, evaporate gradually, and become smaller. But, the data shows that the opposite occurs. What is the reason? Is there something that is missing in the proposed profile? After more analyses, the answer is found in the detailed droplet size distribution plots presented previously in Figs. 4 and 5.

As observed in Fig. 4 for the plot at Y = 10 mm, big droplets do exist as well as the small droplets and the average of the droplet size is about 5 μm, which is consistent with the plot in Fig. 8 (a). It is noted that the peak of the data rate is about 1500 Hz. Now looking downstream at the location X/D = 6 in Fig. 5 for the plot at the same Y at 10 mm, the small droplets that are less than 5 μm takes only a minor portion of the total droplets population. Also, it is noticed that the maximum data rate drops to about 500 Hz. *This means that the smallest droplets dry out faster than the bigger droplets, and, as a result, the total number of droplets decreases and the average droplet size is weighted more towards the bigger droplets.* This explains why the average droplet sizes inside the film increase as it travels downstream. However, this phenomenon only occurs in the early part of the mist's journey (0 < X/D < 6). Downstream from X/D = 6, the droplet sizes and data rates continuously decrease as droplets continuously evaporate and all droplets eventually decrease in size.

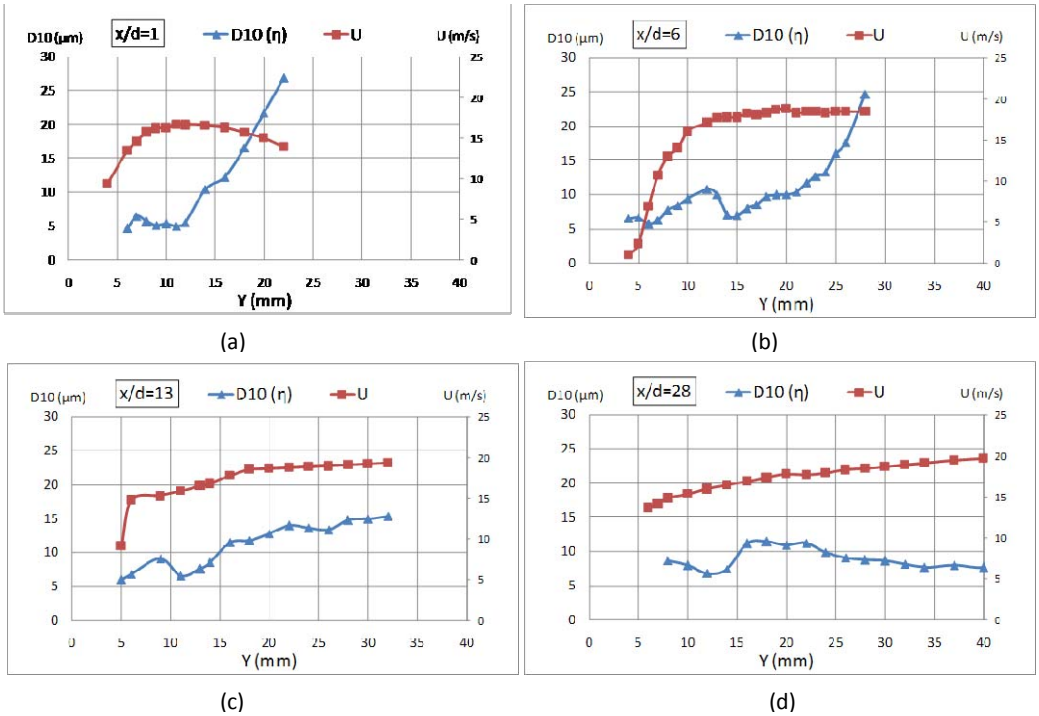

Figure 10 Particle size distribution (plotted on Y-coordinate on the left) and the droplets mean velocity (plotted on Y-coordinate on the right) as a function of Y locations at (a) X/D=1 (b) X/D=6 (c) X/D=13 (d)X/D=28

Now examining the droplet behavior outside the coolant film: for example, looking at the maximum droplet size at Y = 20 mm, the droplet size is observed to be decreasing from X/D = 1 to X/D = 6, which is opposite to that at Y = 10 mm (shown in Fig. 10). *This is also reasonable, because, based on the proposed profile, those droplets are outside the mist/air film layer and only big droplets can reach above the film layer. Therefore, no small droplets are available to begin with, so the droplet sizes only follow a diminishing trend.*

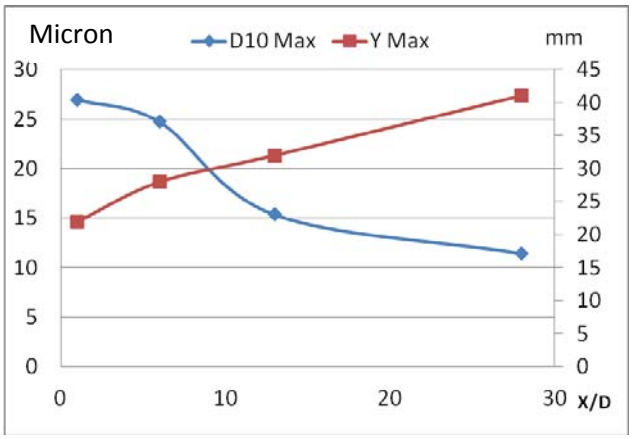

Figure 11 Droplet size distribution on centerline for Case 2, M=0.6

The maximum D_{10} for each X/D location is plotted in Fig.11 and the highest elevations where measurements of droplets are feasible are also plotted in the same figure on the right Y-axis. It is found that the maximum size of droplets is getting smaller as the droplet moves downstream. Meanwhile, the maximum height that the droplets can reach increases as X/D increases.

Based on the description of the thermal-flow physics, the droplet size distribution curves, the droplet data rate distribution curves, and the previous discussions, an illustration of the particle distribution patterns at different locations are drawn in Fig.12.

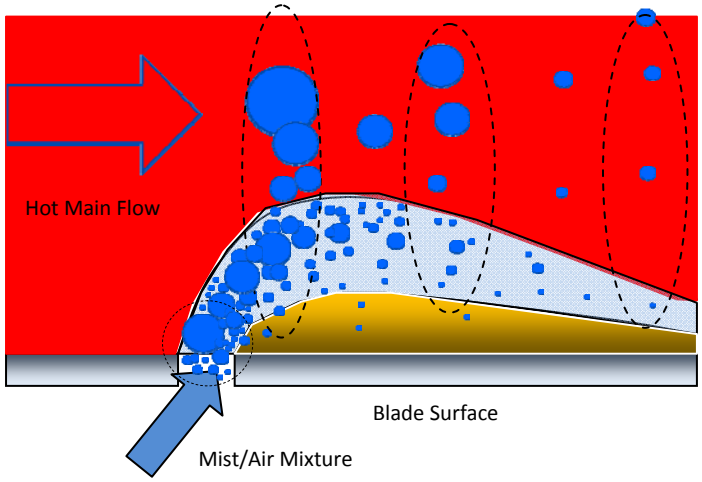

Figure 12 Illustration for droplet distribution profile for low blowing ratio (M=0.6) mist film cooling

Linking the Particle Data with the Heat Transfer Data

Now that the droplet physics have been well examined and are successful in explaining the particle data measurements, efforts will be dedicated to using the knowledge gained for detailed particle behavior to understand the overall heat transfer results. The goal is to find the connection between the droplets' behavior and the heat transfer pattern of mist cooling.

Based on the previous analysis, the shape of the coolant film layer is outlined in Fig. 13 by plotting the upper and lower boundaries of the film layer. It is noted that the plot actually represents the 2-D film layer's center-plane on which the measurements were made. In the experiment, this film layer is actually three-dimensional rather than the two-dimensional plot shown. The lower boundary is plotted according to the data rate curve. The X-axis is the stream-wise location in terms of X/D while the Y-axis is the elevation from the plate surface.

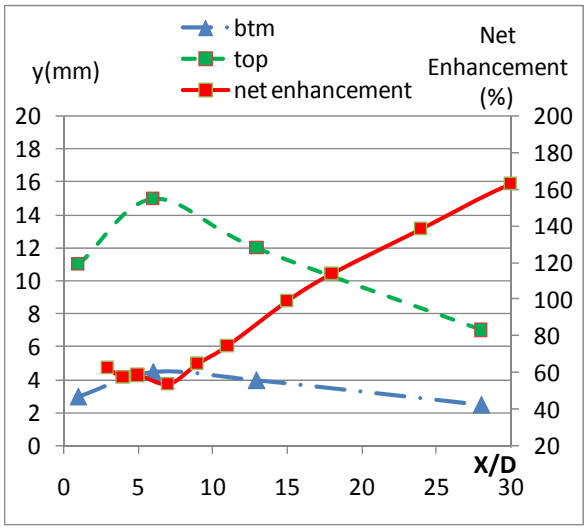

Figure 13 The mid-plane shape of the mist/air coolant film layer for M=0.6 Case at the hole centerline with the Net Enhancement of Cooling Effectiveness plotted on the right Y-axis

As shown in Fig.13, a "bending back" pattern for the mist/air coolant film layer is apparently found at X/D = 7 on the upper boundary of the film. The initial momentum for the jet flow enables the coolant mixture to shoot into the main flow chamber but is bent by the main flow at a certain inclined angle. Since the injection momentum for this case M = 0.6 is not strong enough for the film to be completely lifted off from the surface, the film of air and mist mixture is bent back towards the surface again. The turning point for the film layer is at around X/D = 7 as shown in Fig. 13.

It must be noted here that this detailed description of the film layer shape is only made available with the help of the particle measurement data.

Motivated by the goal of finding the link between the particle behavior and the mist cooling heat transfer, the net enhancement of cooling effectiveness for this case is also plotted in the same figure of the mist/air coolant film sketch in Fig. 13. It is immediately noticed that the starting point of the sudden increase in net enhancement is in the close neighborhood of the "bending back" location of the mist/air film.

This implies that as the mist/air film is bent back and approaches the surface again, the enhancement of cooling effectiveness increases. This "bending back" film pattern is critical in keeping the mist droplets close to the surface, thus improving the cooling effectiveness. It is most important to make sure that the film does not "blow off" in order to have a high cooling enhancement from mist cooling.

CONCLUSION

In this study, an experimental investigation of mist cooling under laboratory conditions is conducted. Mist cooling is evaluated and compared against air film cooling in terms of adiabatic film cooling effectiveness and film coverage.

Through the examination of droplet size distribution, data rate, velocity, and turbulent Reynolds stresses plots, the process of mist interactions with the coolant film is described, and the profile of the coolant film mixture spreading shape is proposed. Characteristics of droplet distribution due to the interaction with both the flow field and temperature field are analyzed. The key points of the physical model are summarized as follows:

1. The coolant air film layer (mixture of cooling air and droplets) does not always coincide with the "droplet layer" (within which droplets reside). Approximately 17% of the droplets are discovered traveling outside the coolant air film.
2. The coolant air film, mixed with the mist droplets, keeps its own identity with distinguishably high Reynolds stresses at the boundaries and also large gradients in the particle size distribution
3. The initial droplet path and distribution are determined mainly by fluid mechanics rather than heat transfer.
4. There is a cold core inside the film layer. The droplet size is bigger within the core and smaller towards both the upper and lower boundaries of the cold core layer.
5. The droplet size decreases faster from the core towards the upper boundary and decays slower towards the lower boundary. As a result, the droplet size population density inside the film skews towards the upper boundary.
6. The droplet population density is higher towards the upper boundary inside the coolant film, but starts to decrease outside the film.
7. Droplets outside the film layer (farther away from the wall) are of larger sizes due to the coolant injecting inertia and a subsequent penetration through the air film layer.
8. The profile of the upper boundary of the air coolant film can be clearly identified from the data rate and droplet size curves. The bottom boundary of the film can be roughly estimated by the location where the data rate is almost below 50Hz.

Based on the above behaviors observed from the experimental measurements, a profile of the "bending back" pattern for the air/mist coolant film is drawn. The bending back location of the mist film layer is at around X/D = 7 with blowing ratio M = 0.6.

A further cross-examination of both the overall heat transfer data and the particle measurements shows that the starting point of the sudden increase in net cooling enhancement is close to the "bending back" location of the mist film. This implies that, as the mist film is bent back and approaches the surface again, the enhancement of cooling effectiveness increases. This "bending back" film pattern is critical in keeping the mist droplets close to the surface, thus improving the cooling effectiveness. It is wise to avoid too strong a blowing ratio so that the film will not lift off of or separate from the surface in order to take full advantage of the higher mist cooling enhancement.

ACKNOWLEDGEMENTS

This study is supported by the Louisiana Governor's Energy Initiative via the Clean Power and Energy Research Consortium (CPERC) and administered by the Louisiana Board of Regents.

REFERENCE

[1] Chaker, M., Meher-Homji, C.B. and Mee, T.R., 2004, "Inlet Fogging of Gas Turbine Engines—Part I: Fog Droplet Thermodynamics, Heat Transfer, and Practical Considerations," Journal of Engineering for Gas Turbines and Power, July 2004, Vol. 126, pp. 545-558.

[2] Young B.W. and. Bachalo W.B, "The Direct Comparison of Three 'In-Flight' Droplet Sizing Techniques for Pesticide Spray Research," International Symposium on Optical Particle Sizing: Theory and Practice, Rouen, France (1987).

[3] Dodge L.G., "Comparison of Performance of Drop-Sizing Instruments," Applied Optics 27:1328-1341 (1987).

[4] Le Coz J.F, "Comparison Of Different Drop Sizing Techniques On Direct Injection Gasoline Sprays," 9th International Symposium On Application Of Laser Techniques To Fluid Mechanics, Lisbon 13-16 July 1998.

[5] W.D. Bachalo, "Method for Measuring the Size and Velocity of Spheres by Dual-Beam Light-Scattering Interferometry," 1980, Applied Optics, Vol. 19, No. 3, pp~ 363-370.

[6] T. Guo, T. Wang, and J.L. Gaddis, "Mist/Steam Cooling in a Heated Horizontal Tube, Part 1: Experimental System, Part 2: Results and Modeling," 2000, ASME J. Turbomachinery, 122, pp. 360–374.

[7] T. Guo, T. Wang, and J.L. Gaddis, "Mist/Steam Cooling in a 180o Tube Bend," 2001, ASME J. Heat Transfer, 122, pp. 749-756.

[8] Wang, T, Gaddis, J. L, and Li, X, "Mist/Steam Heat Transfer of Multiple Rows of Impinging Jets," International Journal of Heat and Mass Transfer v. 48, pp. 5179-5191, 2005

[9] Li, X., Gaddis, J. L., and Wang, T., "Multiple Flow Patterns and Heat Transfer in Confined Jet Impingement," International Journal of Heat and Flow, vol. 26, pp. 746-754, 2005.

[10] Li, X, Gaddis, J. L., and Wang, T, " Mist/Steam Heat Transfer with Jet Impingement onto a Concave Surface," ASME Journal of Heat Transfer, vol. 125, pp.438-446, June, 2003

[11] Li, X, Gaddis, J. L., and Wang, T, " Mist/Steam Cooling by a Row of Impinging Jets," International Journal of Heat and Mass Transfer, 46, pp. 2279-2290, 2003.

[12] Wang, T. and Zhao, L.,"Development of an Experimental Test Facility for Investigating Mist/Air Film Cooling Application in Gas Turbine Airfoils," ASME Paper GT2013-94476, Proceedings of ASME Turbo Expo 2013, San Antonio, Texas, 2013